Derivation of Theoretical Formulas of the Frequency Component Contained in the Overvoltage Related to Long EHV Cables

Ohno, Teruo; Bak, Claus Leth; Ametani, Akihiro; Wiechowski, Wojciech; Kjærsgaard Sørensen, Thomas

Published in:
I E E E Transactions on Power Delivery

DOI (link to publication from Publisher):
10.1109/TPWRD.2011.2179948

Publication date:
2012

Document Version
Early version, also known as pre-print

Derivation of Theoretical Formulas of the Frequency Component Contained in the Overvoltage related to Long EHV Cables

Teruo Ohno, *Member, IEEE*, Claus Leth Bak, *Senior Member, IEEE*, Ametani Akihiro, *Life Fellow, IEEE*
Wojciech Wiechowski, *Senior Member, IEEE* and Thomas Kjærsgaard Sørensen, *Member, IEEE*

***Abstract*—Recent studies of long EHV cables show the importance of performing temporary overvoltage analyses. As the switching of EHV cables can trigger temporary overvoltages, it is important to find the dominant frequency component contained in the switching overvoltages of these cables. Since there are no theoretical formulas to find the dominant frequency, it is generally found by means of time domain simulations or frequency scans. The derivation of theoretical formulas has been desired as the formulas would be useful in verifying the results of time domain simulations or frequency scans. Additionally, the formulas could eliminate the necessity of building simulation models of some network components.**

In order to address this need, this paper derives theoretical formulas to find the dominant frequency in long cable energization overvoltages. The accuracy and practical usefulness of the formulas are confirmed by comparing with the results of time domain simulations.

***Index Terms*—EHV cables, propagation velocity, resonance, temporary overvoltage**

I. Introduction

In recent years, a growing number of transmission line projects has seen the light in many countries throughout the world. The reasons for this are manifold, but include the increase in cross-border trades and renewable energy sources. Until recently, transmission system operators (TSOs) in many countries responded to these necessary transmission upgrades predominantly by introducing overhead lines. HVAC underground cable systems are used, but their use has mainly been limited to densely populated areas. As such, HVAC underground cable systems have until now been limited both in terms of length and number.

This tendency has been changing over the past ten years as the service experience with HVAC, especially EHV AC, cable systems becomes satisfactory to some extent [1]. The use of HVAC cable systems is increasingly proposed in order to protect beautiful landscapes or public health.

Because of this shift in trend, the recently proposed HVAC underground cable systems are longer than existing cable systems [2]–[6]. The longer the cable systems, the lower the frequency contained in the overvoltages associated with cable systems due to their large charging capacity. As low-frequency components are weakly damped, these overvoltages may present challenges that are often ignored in overhead line projects. From the recent studies of long EHV cables, in particular, the authors have found that temporary overvoltages, such as resonance overvoltages, are more severe than slow-front overvoltages and may exceed the insulation strength of related equipment under severe conditions [2]–[5].

Among potential causes of temporary overvoltages, the switching overvoltages of long cables are one of most onerous causes due to its low frequency, as well as the transformer energization. It is therefore important to find the dominant frequency component contained in the switching overvoltage of long cables.

Since theoretical formulas to derive the dominant frequency have not yet been proposed, it has been a common practice to find the dominant frequency through time domain simulations or frequency scans [3]. The derivation of theoretical formulas is expected in order to find or estimate the dominant frequency before such simulations are implemented or to verify the dominant frequency found by these simulations.

Another issue that could be mentioned with regard to temporary overvoltages is the difficulty of the analysis. Generally, severe temporary overvoltages only occur under particular network conditions, and considerable efforts are made in system studies to identify these severe conditions. As the modeling of a broader area is necessary for the temporary overvoltage analysis, it is time-consuming to set up network models and perform time domain simulations or frequency scans in EMT-type programs. As more long cables are being planned or installed, theoretical formulas to derive the dominant frequency are desirable for the efficient planning or operational planning since the theoretical analysis may eliminate the necessity to model some areas of the network.

Nagaoka and Ametani found the impedance and admittance calculation of cross-bonded cables [7]. Based on the impedance and admittance calculation in [7] and [8], this paper derives

Manuscript received January 21, 2011.

Teruo Ohno is with the Tokyo Electric Power Company and the Aalborg University, Aalborg, Denmark (e-mail: ohno.teruo@tepco.co.jp).

Claus Leth Bak is with the Aalborg University, Aalborg, Denmark (e-mail: clb@et.aau.dk).

Akihiro Ametani is with the Doshisha University, Kyoto, Japan (e-mail: aametani@mail.doshisha.ac.jp)

Wojciech Wiechowski is with the WTW Power Solutions, Warsaw, Poland (e-mail: wojciech.wiechowski@wtwps.com).

Thomas Kjærsgaard Sørensen is with the Energinet.dk, Fredericia, Denmark (e-mail: tks@energinet.dk).

theoretical formulas to derive the dominant frequency contained in the switching overvoltage of long cables. The accuracy of the proposed formulas is verified through comparison with time domain simulations.

II. Resonance Overvoltage Analysis

Fig. 1 shows an example of a series resonance overvoltage analysis. When the 400 kV cable line in Fig. 1 is energized, a part of the overvoltage caused by the energization travels through 400 kV transformers to the secondary-side network. The series resonance overvoltage can be caused when the dominant frequency component contained in the energization overvoltage matches the natural frequency of the network composed of 400 kV transformers and the secondary-side network.

The natural frequency (*NF*) can be calculated from the inductance between the primary and secondary windings of the 400 kV transformer and the capacitance of the secondary-side network, assuming that there is no load on the secondary-side network.

$$NF = \frac{1}{2\pi\sqrt{L_{ps}C}} \tag{1}$$

where L_{ps}: inductance of the 400 kV transformer, C: capacitance of the secondary-side network

When there is load on the secondary-side network expressed by inductance (L) and resistance (R) connected in series, the natural frequency can be found as the frequency that minimizes the following magnitude of impedance (X):

$$|X| = \left| R_{ps} + j\omega L_{ps} + \frac{1}{j\omega C + 1/(R + j\omega L)} \right| \tag{2}$$

In general practice, the natural frequency is found by frequency scans, but it is also possible to find the natural frequency from (2) using a mathematics software package.

Equations (1) and (2) indicate that the natural frequency changes depending on the conditions such as the network configuration and load. The resistive part of the load affects the damping of the series resonance overvoltage, and the overvoltage is severe in low-load conditions.

If it is possible to estimate the dominant frequency components contained in the energization overvoltage, it is possible to do without the series resonance overvoltage analysis caused by some lines. As shown in Fig. 1, for example, it is possible to do without the series resonance overvoltage analysis caused by the 400 kV cable line if we can estimate that the dominant frequency in the energization overvoltage is 100 Hz since the natural frequency shown in Fig. 1 is much higher than 100 Hz. In addition, the necessity of modeling the network composed of 400 kV transformers and the secondary-side network may be eliminated.

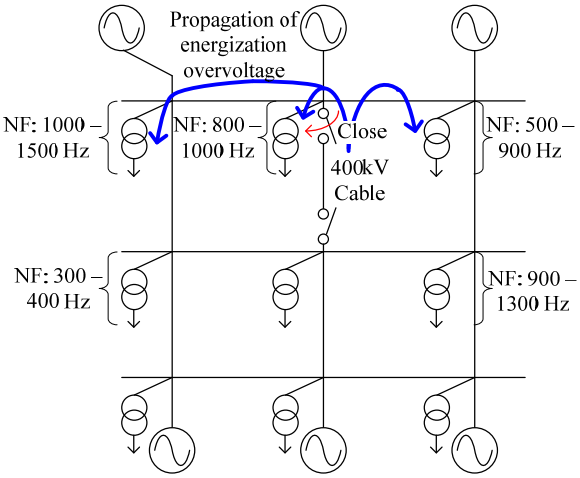

(NF: Natural Frequency)

Fig. 1. Example of a series resonance overvoltage analysis.

However, the theoretical formulas to derive the dominant frequency components have not yet been derived. In the next section, this paper will derive the theoretical formulas with the focus on long cables since its energization overvoltage contains lower-frequency components, which leads to severe conditions, namely low damping in the network.

This section shows an example of a series resonance overvoltage analysis with the network illustrated in Fig. 2. The loading condition was set to 142.6 MW + *j*67.19 MVar by setting R = 100 ohm and L = 150 mH. The network shown in Fig. 1 was simplified to Fig. 2 in order to compare with the theoretical analysis in the following sections.

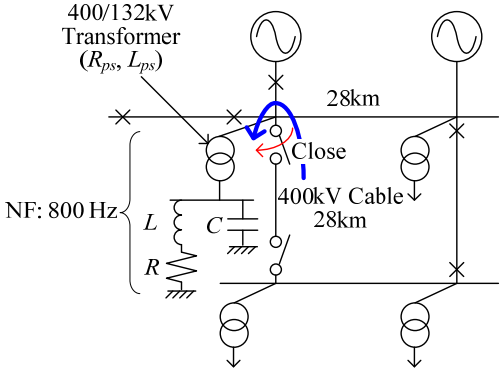

400/132 kV transformer: *Rps* = 8 ohm, *Lps* = 1916 mH (at 400 kV), 132 kV network: R = 100 ohm, L = 150 mH, C = 2.16 μF

Fig. 2. Simple simulation circuit for the series resonance overvoltage analysis.

First, it is necessary to find the dominant frequency contained in the energization overvoltage. The objective of this paper is the derivation of the dominant frequency without performing time domain simulations, but here, as in general practice, the time domain simulation of the cable energization was conducted to find the dominant frequency. Cable data used in the simulation are described in Section IV.

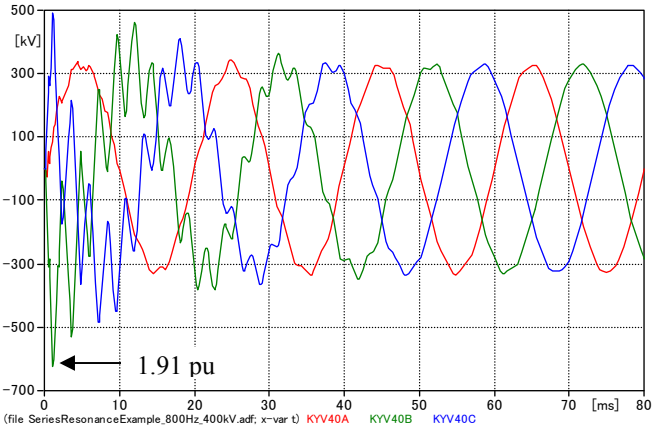

Fig. 3. Results of the cable energization overvoltage analysis.

Fig. 4 shows the result of the Fourier analysis of the voltage waveform in Fig. 3. As the cable energization overvoltage is almost damped by 40 ms, the time window of the Fourier transform is set to 0 – 40 ms. The figure shows that the dominant frequency contained in the cable energization overvoltage is 425 Hz.

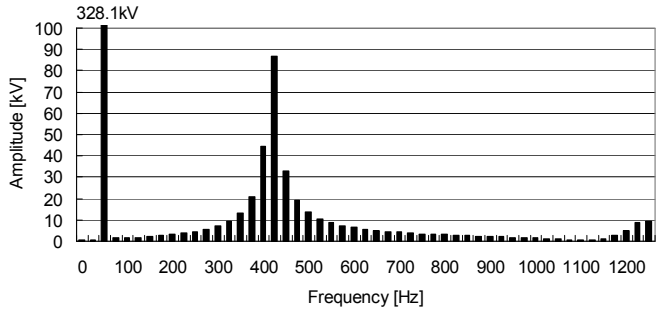

Fig. 4. Results of the Fourier analysis of the cable energization overvoltage.

Fig. 5 shows the voltage waveform at the LV side of the transformer. As no series resonance occurs, the overvoltage is almost at the same level as that shown in Fig. 3 (HV side).

In Fig. 5, the natural frequency of the network composed of the 400 kV transformer and the 132 kV network was 800 Hz, which is far from the dominant frequency in the energization overvoltage (425 Hz). In order to excite the series resonance, the natural frequency was shifted to 425 Hz by increasing the capacitance in the 132 kV network to 7.6 μF. The value of the capacitance was found by performing frequency scans.

Fig. 6 shows the voltage waveform on the LV side of the transformer. When comparing this waveform with the one shown in Fig. 3 (HV side), it becomes clear that the overvoltage is amplified on the LV side due to the series resonance since the natural frequency was set exactly at the dominant frequency. The Fourier analysis of the voltage waveform in Fig. 6 demonstrates that the dominant frequency contained in the series resonance overvoltage is 425 Hz and matches the cable energization overvoltage.

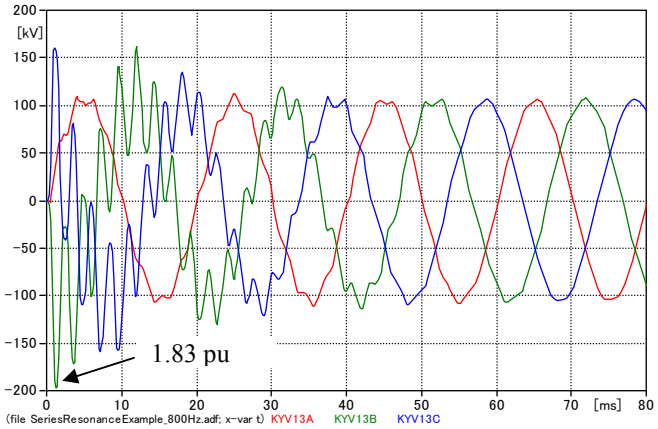

Fig. 5. Results of the series resonance overvoltage analysis (NF = 800 Hz).

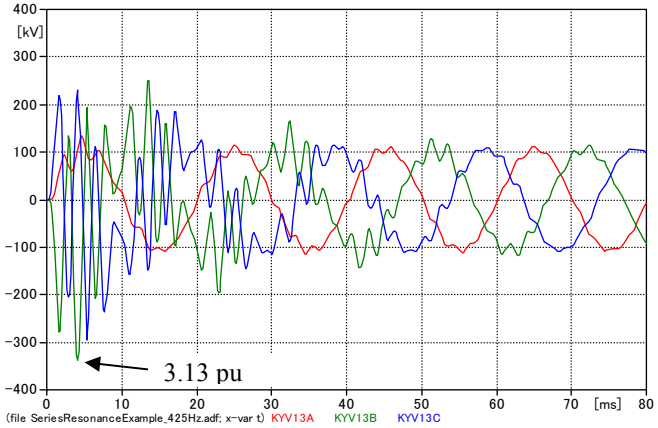

Fig. 6. Results of the series resonance overvoltage analysis (natural frequency is adjusted to 425 Hz).

The time domain simulations were performed with different natural frequencies by changing the capacitance in the 132 kV network. Fig. 7 shows that the series resonance overvoltage becomes more severe when the natural frequency becomes closer to 425 Hz.

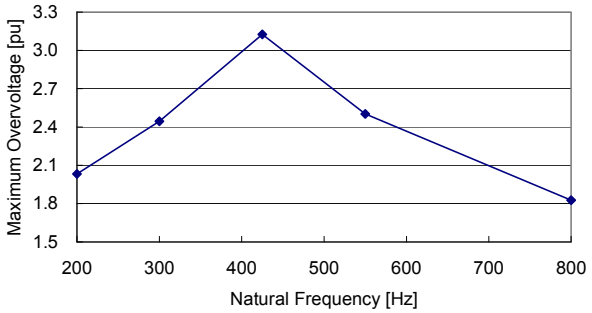

Fig. 7. Effect of the natural frequency on the series resonance overvoltage.

The example given in this section illustrates the importance of understanding the natural frequency of the network and the dominant frequency in the energization overvoltage. Finding the possible range of the natural frequency of the network using (1) or (2) is fairly straightforward. The theoretical formulas of the dominant frequency in the energization overvoltage are derived in the following section.

III. Derivation of Theoretical Formulas to Estimate Dominant Frequency

A. Average Impedance and Admittance

The metallic sheath of long cables is generally cross-bonded in order to reduce both sheath induced current and sheath voltage.

Cross-bonding has been found to affect cable impedance and admittance, and their derivation is given in [7] and [8].

Assuming that each minor section of a cable is of equal length, the average impedance of the cross-bonded cable for one major section is given by the following equation.

$$[Z] = ([z] + [R][z][R]^{-1} + [R]^{-1}[z][R]) / 3 \tag{3}$$

Here, $[z]$ is the impedance of the cable per unit length for one minor section, and $[R]$ is the rotation matrix.

$$[z] = \begin{bmatrix} [z_{CoCo}] & [z_{CoSh}] \\ [z_{CoSh}] & [z_{ShSh}] \end{bmatrix} \tag{4}$$

$$[R] = \begin{bmatrix} 1 & 0 & 0 & 0 & 0 & 0 \\ 0 & 1 & 0 & 0 & 0 & 0 \\ 0 & 0 & 1 & 0 & 0 & 0 \\ 0 & 0 & 0 & 0 & 0 & 1 \\ 0 & 0 & 0 & 1 & 0 & 0 \\ 0 & 0 & 0 & 0 & 1 & 0 \end{bmatrix} \tag{5}$$

where $[z_{CoCo}]$: impedance between conductors
$[z_{CoSh}]$: impedance between conductors and sheaths
$[z_{ShSh}]$: impedance between sheaths

The calculation of the average impedance of one major section, as shown in Fig. 8, yields the following equations.

$$[Z] = \begin{bmatrix} [Z_{CoCo}] & [Z_{CoSh}] \\ [Z_{CoSh}]^T & [Z_{ShSh}] \end{bmatrix} \tag{6}$$

$$[Z_{CoCo}] = [z_{CoCo}] \tag{7}$$

$$[Z_{CoSh}] = \begin{bmatrix} Z_{AS} & Z_{AS} & Z_{AS} \\ Z_{BS} & Z_{BS} & Z_{BS} \\ Z_{CS} & Z_{CS} & Z_{CS} \end{bmatrix} \tag{8}$$

$$[Z_{ShSh}] = \begin{bmatrix} Z_{SS} & Z_{SM} & Z_{SM} \\ Z_{SM} & Z_{SS} & Z_{SM} \\ Z_{SM} & Z_{SM} & Z_{SS} \end{bmatrix} \tag{9}$$

Impedances in (8) and (9) are given by

$$\begin{cases} Z_{AS} = (z_{Aa} + z_{Ab} + z_{Ac}) / 3 \\ Z_{BS} = (z_{Ba} + z_{Bb} + z_{Bc}) / 3 \\ Z_{CS} = (z_{Ca} + z_{Cb} + z_{Cc}) / 3 \\ Z_{SS} = (z_{aa} + z_{bb} + z_{cc}) / 3 \\ Z_{SM} = (z_{ab} + z_{bc} + z_{ca}) / 3 \end{cases} \tag{10}$$

In subscripts of impedances, uppercase letters show the phase of the conductor while lowercase letters show the phase of the metallic sheath.

Similarly, the average admittance of the cross-bonded cable for one major section can be calculated as follows:

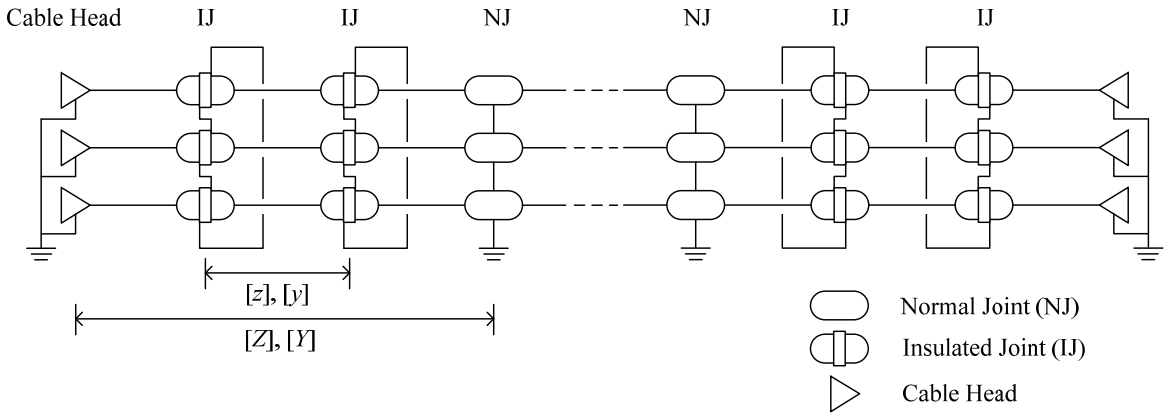

Fig. 8. Cross-bonding diagram.

$$[Y] = ([y] + [R][y][R]^{-1} + [R]^{-1}[y][R]) / 3 = \begin{bmatrix} [Y_{CoCo}] & [Y_{CoSh}] \\ [Y_{CoSh}] & [Y_{ShSh}] \end{bmatrix} \quad (11)$$

$$[Y_{CoCo}] = y_{AA} \cdot I \quad (12)$$

$$[Y_{CoSh}] = -\frac{y_{AA}}{3}\begin{bmatrix} 1 & 1 & 1 \\ 1 & 1 & 1 \\ 1 & 1 & 1 \end{bmatrix} \quad (13)$$

$$[Y_{ShSh}] = y_{SS} \cdot I \quad (14)$$

In (12) and (14), I is the identity matrix.

Since the metallic sheath of the cross-bonded cable is earthed at both ends of a major section, $[Z]$ and $[Y]$ can be reduced to 4 x 4 matrices. The reduction is, however, not performed as the dominant frequency can be found in a simpler form without the matrix reduction.

B. Derivation of Theoretical Formulas

The main focus of this paper is to find the dominant frequency from $[Z]$ and $[Y]$ by means of simple theoretical formulas. For a given length of a line, one propagation velocity is linked to one dominant frequency by (15). The relationship can be found, remembering that the current is zero at the open terminal, as the fundamental resonance frequency from the general solution of the set of wave equations given by d'Alembert in 1750's.

$$f_i = \frac{1}{4\tau} = \frac{v_i}{4 \times (\text{line length})} \quad (15)$$

Thus, we need to find the propagation velocity of the dominant frequency component in simple theoretical formulas.

It is known that the propagation velocity of each mode is found by (16) [9].

$$v_i = \frac{2\pi f_0}{\mathrm{Im}(\sqrt{z_i y_i})} \quad (16)$$

Here, z_i and y_i are i-th diagonal entries of the modal impedance matrix $[Z_M]$ and the admittance matrix $[Y_M]$, respectively. The imaginary part of $\sqrt{z_i y_i}$ is denoted by $\mathrm{Im}(\sqrt{z_i y_i})$. f_0 is the target frequency. ($i = 1, 2, \cdots, 6$)

Equation (16) can also be expressed in a compact form as

$$(v) = diag\left(\frac{2\pi f_0}{\mathrm{Im}(\sqrt{[Z_M][Y_M]})}\right) \quad (17)$$

Modal impedance and admittance matrices can be found by diagonalizing $[Z]$ and $[Y]$, but the diagonalization process prohibits the derivation of theoretical formulas in simple form. It is necessary to find $[Z_M][Y_M]$ from $[Z]$ and $[Y]$ without conducting diagonalization.

The relationship between voltage (V) and current (I) in a distributed parameter line can be expressed as

$$\frac{d(V)}{dx} = -[Z](I) \quad (18)$$

From the definition of voltage and current transformation matrices,

$$[T_v]\frac{d(v)}{dx} = -[Z][T_i](i) \quad (19)$$

where (v) and (i) are voltage and current in a distributed parameter line in a modal domain.

Multiplying both sides of (19) from the left by $[T_v]^{-1}$,

$$\frac{d(v)}{dx} = -[T_v]^{-1}[Z][T_i](i) \quad (20)$$

From the definition of the modal impedance matrix and with similar calculation for the modal admittance matrix,

$$[Z_M] = [T_v]^{-1}[Z][T_i], [Y_M] = [T_i]^{-1}[Y][T_v] \quad (21)$$

Here, $[T_v]$ and $[T_i]$ are voltage and current transformation matrices.

The product $[Z_M][Y_M]$ can be calculated as

$$[Z_M][Y_M] = \left([T_v]^{-1}[Z][T_i]\right)\left([T_i]^{-1}[Y][T_v]\right) = [T_v]^{-1}[Z][Y][T_v] = [D] \quad (22)$$

where $[D]$ is the eigenvalue matrix of $[Z][Y]$.

Equation (22) shows that the entries of $[Z_M][Y_M]$ can be found from the eigenvalues of $[Z][Y]$.

Using (6) to (14), the matrix $[Z][Y]$ is given as

$$[Z][Y] = \begin{bmatrix} F_{11}y_{AA} & F_{12}y_{AA} & F_{13}y_{AA} & F_{AX} & F_{AX} & F_{AX} \\ F_{21}y_{AA} & F_{22}y_{AA} & F_{23}y_{AA} & F_{BX} & F_{BX} & F_{BX} \\ F_{31}y_{AA} & F_{32}y_{AA} & F_{33}y_{AA} & F_{CX} & F_{CX} & F_{CX} \\ F_{AY} & F_{BY} & F_{CY} & F_{SS} & F_{SM} & F_{SM} \\ F_{AY} & F_{BY} & F_{CY} & F_{SM} & F_{SS} & F_{SM} \\ F_{AY} & F_{BY} & F_{CY} & F_{SM} & F_{SM} & F_{SS} \end{bmatrix} \quad (23)$$

Here, variables $F_{11}, F_{12}, \cdots, F_{33}$ in the upper left 3-by-3 entries can be calculated as

$$\begin{cases} F_{11} = z_{AA} - Z_{AS}, \ F_{12} = z_{AB} - Z_{AS}, \ F_{13} = z_{CA} - Z_{AS} \\ F_{21} = z_{AB} - Z_{BS}, \ F_{22} = z_{AA} - Z_{BS}, \ F_{23} = z_{BC} - Z_{BS} \\ F_{31} = z_{CA} - Z_{CS}, \ F_{32} = z_{BC} - Z_{CS}, \ F_{33} = z_{AA} - Z_{CS} \end{cases} \tag{24}$$

where Z_{AS}, Z_{BS}, and Z_{CS} are given by (10).

In the upper right 3-by-3 entries,

$$F_{AX} = -(z_{AA} + z_{AB} + z_{CA}) y_{AA} / 3 + Z_{AS} y_{SS} \tag{25}$$

F_{BX} and F_{CX} can be found similarly.

In the lower left 3-by-3 entries,

$$F_{AY} = Z_{AS} y_{AA} - (Z_{SS} + 2Z_{SM}) y_{AA} / 3 \tag{26}$$

F_{BY} and F_{CY} can be found similarly.

In the lower right 3-by-3 entries,

$$F_{SS} = -(Z_{AS} + Z_{BS} + Z_{CS}) y_{AA} / 3 + Z_{SS} y_{SS} \tag{27}$$

$$F_{SM} = -(Z_{AS} + Z_{BS} + Z_{CS}) y_{AA} / 3 + Z_{SM} y_{SS} \tag{28}$$

Instead of diagonalizing $[Z][Y]$, this paper assumes that the overvoltage caused by the energization of a long cross-bonded cable is dominated by inter-phase modes. Under this assumption, the eigenvectors of inter-phase modes are found in an ideal form and it is possible to find the theoretical formulas in a simple form which does not require matrix computation software. In order for the coaxial mode to dominate the energization overvoltage, the dominant frequency must be higher than the critical frequency given by (29) [10][11].

$$f_c \approx \rho_s / \pi \mu_s d^2 \tag{29}$$

where ρ_s is sheath resistivity, μ_s is sheath permeability, and d is sheath thickness.

The critical frequency calculated by (29) for a typical 400 kV XLPE cable ranges from 1000 – 1500 Hz. It is therefore reasonable to assume that inter-phase modes dominate the energization overvoltage, since the dominant frequency, which is higher than this critical frequency, cannot be originated from long cross-bonded cables.

Since the ideal eigenvector of the first inter-phase mode is known as $T_{V1} = (-1/3 \ \ 2/3 \ \ -1/3 \ \ 0 \ \ 0 \ \ 0)^T$, the eigenvalue corresponding to this inter-phase mode can be found as

$$\begin{aligned} D_1 &= -(2z_{AB} - z_{AA} - z_{CA}) y_{AA} \quad \text{or} \\ &= (2z_{AA} - z_{AB} - z_{BC}) y_{AA} / 2 \end{aligned} \tag{30}$$

The eigenvalue corresponding to the second inter-phase mode $T_{V2} = (1/2 \ \ 0 \ \ -1/2 \ \ 0 \ \ 0 \ \ 0)^T$ is calculated as

$$D_2 = (z_{AA} - z_{CA}) y_{AA} \tag{31}$$

Once the eigenvalues are found by (30) and (31), the propagation velocities are found by

$$v_i = 2\pi f_0 / \mathrm{Im}(\sqrt{D_i}) \tag{32}$$

(f_0: target frequency, i = 1, 2)

Equations (30) – (32) indicate that simple readily available data will provide the estimation of dominant frequency.

C. Effect of Source Impedance

Theoretical formulas have so far been derived assuming there is no source impedance. This may be justified in the slow-front overvoltage analysis as source impedance changes depending on network conditions and no source impedance is supposedly the most severe condition.

This section considers the effect of source impedance since it affects the dominant frequency. The amplitude of the overvoltage caused by cable line energization will be mitigated by the introduction of source impedance, but also the lowered dominant frequency may cause resonances and lead to higher resonance overvoltages.

First, when the source impedance is given as lumped parameter impedance Z_0, it has to be converted to distributed parameter source impedance z_0 by (33). Fig. 9 illustrates the reason why the conversion is necessary. By the conversion, the lumped parameter source impedance can be considered a part of the distributed parameter cable line. The dominant frequency for the distributed parameter model can be derived from (15) and (16).

$$z_0 = Z_0 \times \left(\frac{2\pi}{4} \right)^2 \tag{33}$$

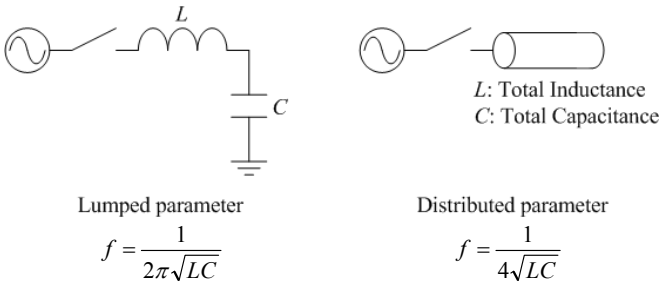

Fig. 9. Comparison of dominant frequency.

Assuming that the source impedance is a part of the cable line, the eigenvalues corresponding to the two inter-phase modes are found as:

$$\begin{aligned} D_1 &= \{z_0 - (2z_{AB} - z_{AA} - z_{AC})\} y_{AA} \quad \text{or} \\ &= (z_0 + 2z_{AA} - z_{AB} - z_{BC}) y_{AA} / 2 \end{aligned} \tag{34}$$

$$D_2 = (z_0 + z_{AA} - z_{AC}) y_{AA} \tag{35}$$

When the eigenvalues have been found, the propagation velocity and dominant frequency can be calculated by (32) and (15).

IV. Comparison with EMTP Simulations

In order to confirm the accuracy of the formulas derived in the previous section, dominant frequencies are derived through theoretical formulas and time domain simulations in a simple cable energization example. The comparison of these dominant frequencies shows the accuracy of the formulas derived.

A planned cable line in Denmark is used as the simple cable energization example together with the Danish network. Fig. 10 shows the planned 400 kV cable line from the substation ASV to KYV via TOR. The cable line is being planned by the Danish TSO, Energinet.dk, and it is necessary to make sure that the switching of this cable line does not cause series resonance overvoltages at ASV or KYV. As discussed in the previous section, the prior knowledge of the dominant frequency offered by the theoretical formulas is useful for the series resonance overvoltage analysis.

Fig. 10. The planned 400 kV ASV – TOR – KYV cable line in the Eastern Danish grid (courtesy of Energinet.dk).

It has not been determined yet whether the TOR substation will have switchgears for the cable line or not. Under the assumption that TOR is equipped with switchgears, the simple cable energization example was performed with the planned ASV – TOR cable line according to the single line diagram in Fig. 11. The whole 400 kV Eastern Danish grid was modeled in PSCAD for the simple cable energization example. Fig. 11 shows the simulation model setup only near ASV. The length of the ASV – TOR cable line is approximately 28 km, and the cable line was energized from the ASV side.

Fig. 12 shows physical and electrical data for the 400 kV Al 1600 mm^2 XLPE cable, which is one of the candidates for the ASV – TOR cable line. Relative permittivity of the insulation was adjusted using (36) to set the accurate admittance for the cable.

$$\varepsilon I1 = \frac{\ln(R3/R2)}{\ln(Rso/Rsi)}\varepsilon I0 = \frac{\ln(58.0/26.0)}{\ln(55.0/28.0)}\cdot 2.4 = 2.852 \qquad (36)$$

where

Rsi: Outer radius of conductor screen, Rso: Outer radius of the insulation, $\varepsilon I0$: relative permittivity of the insulation, $\varepsilon I1$: adjusted relative permittivity of the insulation

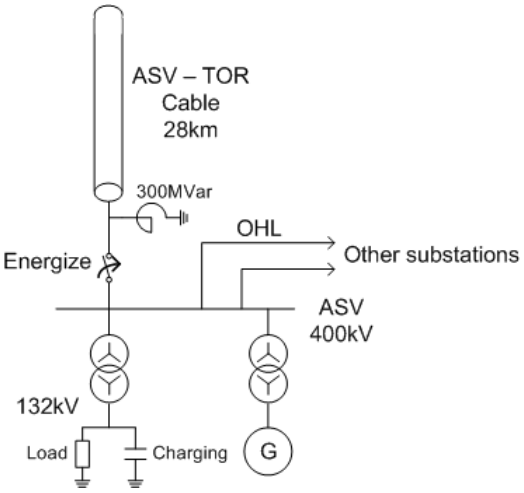

Fig. 11. Energization setup for ASV – TOR cable line.

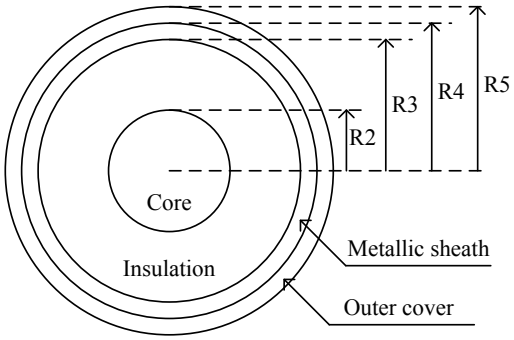

R2 = 2.60 cm, R3 = 5.80 cm, R4 = 5.92 cm, R5 = 6.35 cm
Core inner radius: 0.0 cm, Core resistivity: 2.84×10^{-8} Ωm,
Metallic sheath resistivity: 2.840×10^{-8} Ωm,
Relative permittivity (XLPE, PE): 2.4

Fig. 12. Physical and electrical data of the cable.

Fig. 13 displays the cable layout. It was assumed that the cable was directly buried at a depth of 1.3 m with a horizontal separation of 0.3 m.

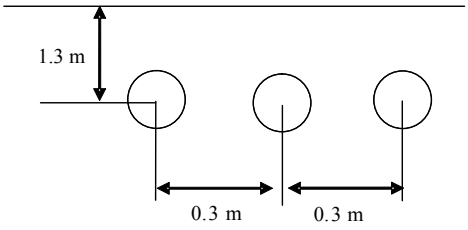

Fig. 13. Cable layout.

First, the dominant frequencies were calculated using the theoretical formulas derived in Section II. The calculation was based on the future off-peak condition when the ASV – KYV cable line is installed. In this off-peak condition, the fault current level at the ASV 400 kV bus was found to be 10.3 kA

by simulating a three-phase short-circuit fault in PSCAD. In order to consider the effect of source impedance, the dummy generator was connected to the 400 kV ASV bus. The source impedance of the dummy generator was changed from 0.1 mH to infinite (no dummy generator).

In order to derive the dominant frequency, it is necessary to find the cable impedance and admittance for one minor section. These were obtained using CABLE CONSTANTS in EMTP as shown in the Appendix. The Appendix also shows an average impedance $[Z]$ and admittance $[Y]$ of the cross-bonded cable, derived from (3) and (11), and $[Z][Y]$.

As a result of the calculation, the mode transformation matrix of $[Z][Y]$ is found as:

$[T_V]$

0.40343	0.50033	-0.29561	-0.41764	0.70710	0.57058
0.41761	0	0.57115	0.80692	0	0.59064
0.40343	-0.50033	-0.29561	-0.41764	-0.70710	0.57058
0.40349	0.49949	-0.29477	0	0	0
0.41768	0	0.56942	0	0	0
0.40349	-0.49949	-0.29477	0	0	0

Comparing $[T_V]$ with T_{V1} and T_{V2}, the mode transformation matrix contains ideal eigenvectors for inter-phase modes, which coincides with the assumption used in the derivation of theoretical formulas.

Equations (32), (34), (35), and (15) yield propagation velocities and dominant frequencies. Table I shows the propagation velocities and dominant frequencies obtained for different fault current levels. Only the inductance part is used as impedance in the calculation.

The impedance and admittance matrices in the Appendix were calculated at 850 Hz, which was near the dominant frequency when dummy source impedance was 0.1 mH. When the identified dominant frequency is far from 850 Hz, it is possible to re-calculate impedance matrices at the identified dominant frequency and update the dominant frequency (second trial). However, since the frequency dependence of inductances that are used for the calculation of the dominant frequency is quite small over the frequency range of interest as shown in Fig. 14, it is, in general, possible to achieve satisfactory accuracy without the second trial. In this example, the second trial led to the improvement of 0.4 Hz or lower.

TABLE I
DOMINANT FREQUENCIES DERIVED THROUGH PROPOSED FORMULAS

Source impedance [mH] (dummy)	0.1	50	100	200	No dummy
Network Source Impedance [mH]	0.1	24.5	37.5	51.0	71.4
Propagation velocity [m/μs]					
mode 1	100.5	44.7	37.1	32.2	27.5
mode 2	89.0	42.5	35.8	31.4	27.0
average	94.8	43.6	36.4	31.8	27.2
Dominant frequency [Hz]	846.0	389.3	325.4	283.9	243.4

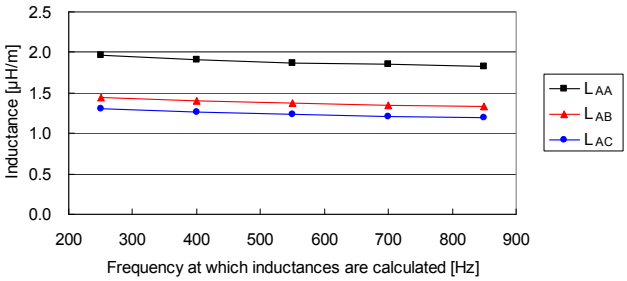

L_{AA}, L_{AB}, L_{AC}: inductance part of Z_{AA}, Z_{AB}, Z_{AC}

Fig. 14. Frequency dependence of inductances used for the calculation of dominant frequencies.

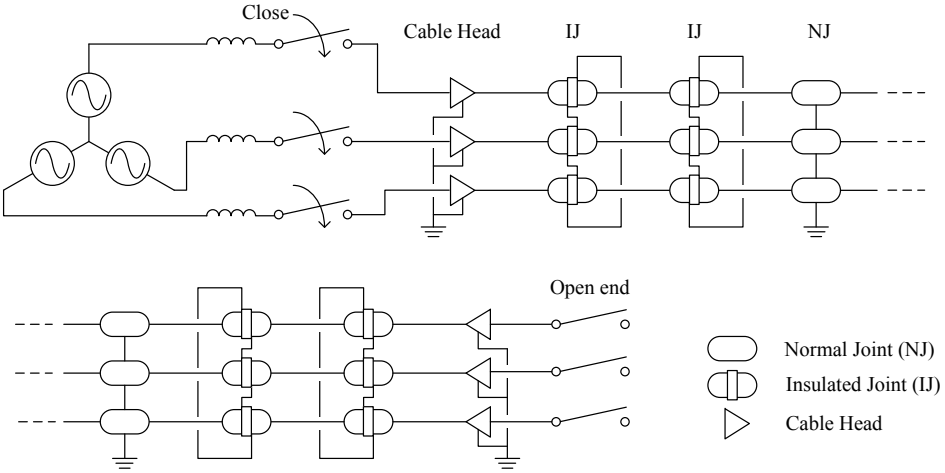

Fig. 15. Implementation of the cable model with PSCAD.

Second, the dominant frequencies were obtained through EMTP simulations. All conditions were kept equal to the theoretical derivation. Fig. 15 shows how the cable was modeled using PSCAD. The cable was modeled using the frequency dependent (phase) model. The cable was cross-bonded, and the length of the minor section was set to 1.867 km. As the total cable length is 28 km, the cable has 15 minor sections.

It was assumed that surge arresters were installed at the primary terminal of the transformer and 400 kV overhead line feeders connected to the ASV 400 kV bus. Table II shows the V-I characteristic of the surge arrester.

TABLE II
V-I CHARACTERISTIC OF SURGE ARRESTER

I [A]	V [V]
1.0E-03	4.81E+05
1.0E-02	5.09E+05
1.0E-01	5.44E+05
1.0E+00	5.78E+05
1.0E+01	6.13E+05
1.0E+02	6.47E+05
5.0E+02	6.84E+05
1.0E+03	7.04E+05
2.0E+03	7.32E+05
5.0E+03	7.75E+05

Fig. 16 shows the voltage at the open terminal (TOR) of the cable during cable energization. The source impedance of the dummy generator was set to 100 mH in this example. Dominant frequencies were obtained by applying the Fourier analysis to the voltage waveform. The simulation was repeated with different magnitudes of the source impedance to find dominant frequencies for different fault current levels.

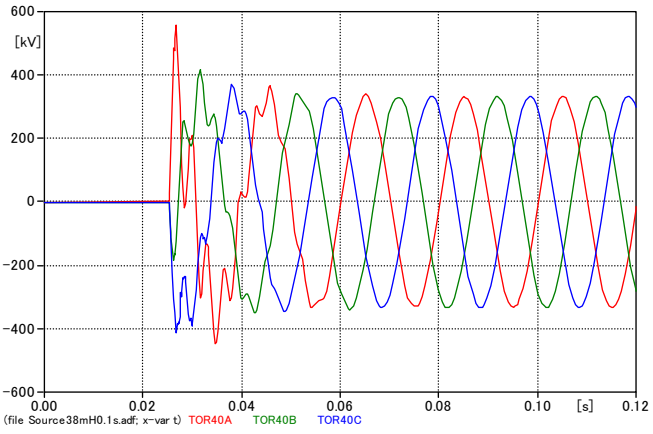

Fig. 16. Voltage waveforms at the open terminal during cable energization (dummy source impedance: 100 mH).

Fig. 17 shows the result of the Fourier analysis of the voltage waveforms in Fig. 16. The time window of the Fourier transform starts from the arrival of the overvoltage at the open terminal (0.025 ms) and ends after one cycle (0.045 ms). The result shows that the dominant frequency exists near 300 Hz.

In order to obtain the dominant frequency more precisely, the window size of the Fourier transform is extended to 0.1 s in Fig. 18. The extended window size enables to find the magnitude of each frequency component by 10 Hz step. The figure shows that the dominant frequency is located at 310 Hz.

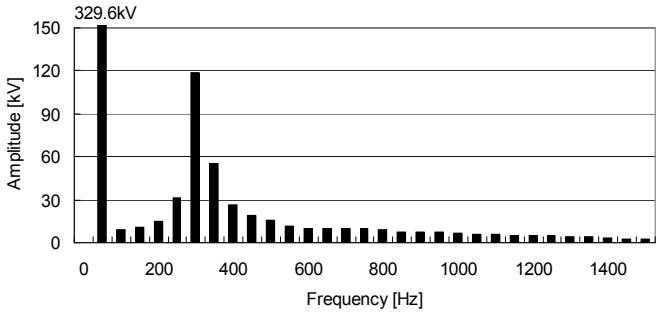

Fig. 17. Results of the Fourier analysis of the voltage waveforms at the open terminal in the cable energization (dummy source impedance: 100 mH, 50 Hz step)

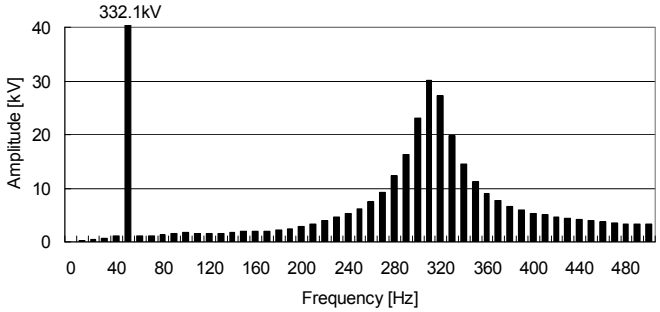

Fig. 18. Results of the Fourier analysis of the voltage waveforms at the open terminal in the cable energization (dummy source impedance: 100 mH, 10 Hz step)

Fig. 19 illustrates the comparison of dominant frequencies derived through theoretical formulas and those found by EMTP simulations. The comparison shows that the theoretical formulas derived have a very high accuracy.

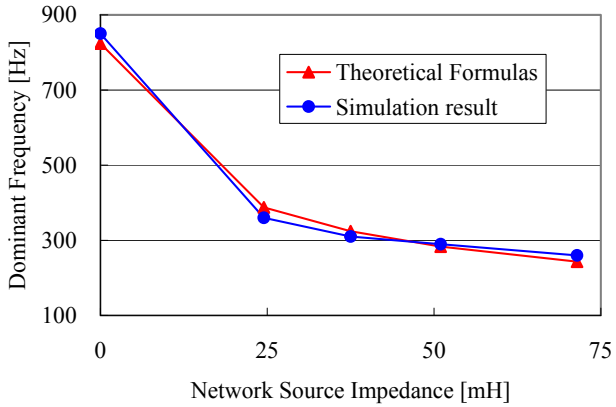

Fig. 19. Comparison of dominant frequencies found through theoretical formulas and EMTP simulations.

V. Conclusion

Simple theoretical formulas for estimating the propagation velocity and dominant frequency were derived from impedance and admittance calculations. The comparison between the proposed formulas and the simulation results was performed using the planned Danish 400 kV cable line as an example. From the comparison, the derived formulas were found to be sufficiently accurate to be used for the efficient analysis of resonance overvoltages. In addition, the accuracy of the formulas derived demonstrates that the propagation velocity and the dominant frequency are determined by two inter-phase modes for long cables.

In the example, an average of two propagation velocities corresponding to two inter-phase modes were used to derive the theoretical dominant frequency, assuming an equal contribution from two inter-phase modes. This assumption resulted in the excellent accuracy in the example, but the verification of the validity of the assumption should be categorized as a future challenge.

Appendix:

Impedance and admittance matrices for the ASV – KYV cable in Section IV are found as follows for one minor section using CABLE CONSTANTS:

$[z]$ (upper: R, lower: ωL)

0.000892967	0.000829102	0.000829084	0.000829417	0.000829102	0.000829084
0.009758371	0.007086453	0.006346075	0.008830749	0.007086453	0.006346075
0.000829102	0.000892967	0.000829102	0.000829102	0.000829417	0.000829102
0.007086453	0.009758371	0.007086453	0.007086453	0.008830749	0.007086453
0.000829084	0.000829102	0.000892967	0.000829084	0.000829102	0.000829417
0.006346075	0.007086453	0.009758371	0.006346075	0.007086453	0.008830749
0.000829417	0.000829102	0.000829084	0.00089355	0.000829102	0.000829084
0.008830749	0.007086453	0.006346075	0.008827109	0.007086453	0.006346075
0.000829102	0.000829417	0.000829102	0.000829102	0.00089355	0.000829102
0.007086453	0.008830749	0.007086453	0.007086453	0.008827109	0.007086453
0.000829084	0.000829102	0.000829417	0.000829084	0.000829102	0.00089355
0.006346075	0.007086453	0.008830749	0.006346075	0.007086453	0.008827109

$[y]$ (ωC)

1.05612E-06	0	0	-1.0561E-06	0	0
0	1.05612E-06	0	0	-1.0561E-06	0
0	0	1.05612E-06	0	0	-1.0561E-06
-1.0561E-06	0	0	1.12258E-05	0	0
0	-1.0561E-06	0	0	1.12258E-05	0
0	0	-1.0561E-06	0	0	1.12258E-05

Average impedance and admittance matrices for the ASV – KYV cable are calculated by (3) and (11), considering cross-bonding:

$[Z]$

0.000892967	0.000829102	0.000829084	0.000829201	0.000829201	0.000829201
0.009758371	0.007086453	0.006346075	0.007421093	0.007421093	0.007421093
0.000829102	0.000892967	0.000829102	0.000829207	0.000829207	0.000829207
0.007086453	0.009758371	0.007086453	0.007667885	0.007667885	0.007667885
0.000829084	0.000829102	0.000892967	0.000829201	0.000829201	0.000829201
0.006346075	0.007086453	0.009758371	0.007421093	0.007421093	0.007421093
0.000829201	0.000829207	0.000829201	0.00089355	0.000829096	0.000829096
0.007421093	0.007667885	0.007421093	0.008827109	0.00683966	0.00683966
0.000829201	0.000829207	0.000829201	0.000829096	0.00089355	0.000829096
0.007421093	0.007667885	0.007421093	0.00683966	0.008827109	0.00683966
0.000829201	0.000829207	0.000829201	0.000829096	0.000829096	0.00089355
0.007421093	0.007667885	0.007421093	0.00683966	0.00683966	0.008827109

$[Y]$

1.0561E-06	0	0	-3.5204E-07	-3.5204E-07	-3.5204E-07
0	1.0561E-06	0	-3.5204E-07	-3.5204E-07	-3.5204E-07
0	0	1.0561E-06	-3.5204E-07	-3.5204E-07	-3.5204E-07
-3.5204E-07	-3.5204E-07	-3.5204E-07	1.1226E-05	0	0
-3.5204E-07	-3.5204E-07	-3.5204E-07	0	1.1226E-05	0
-3.5204E-07	-3.5204E-07	-3.5204E-07	0	0	1.1226E-05

$[Z][Y]$

-2.4685E-09	3.5342E-10	1.1354E-09	-7.5143E-08	-7.5143E-08	-7.5143E-08
6.7345E-11	-1.0467E-13	-1.2314E-13	8.4103E-09	8.4103E-09	8.4103E-09
6.1406E-10	-2.2078E-09	6.1406E-10	-7.7653E-08	-7.7653E-08	-7.7653E-08
-1.1082E-13	6.7339E-11	-1.1082E-13	8.4104E-09	8.4104E-09	8.4104E-09
1.1354E-09	3.5342E-10	-2.4685E-09	-7.5143E-08	-7.5143E-08	-7.5143E-08
-1.2314E-13	-1.0467E-13	6.7345E-11	8.4103E-09	8.4103E-09	8.4103E-09
8.5600E-11	-1.7504E-10	8.5600E-11	-9.1167E-08	-6.8856E-08	-6.8856E-08
-2.2580E-11	-2.2573E-11	-2.2580E-11	9.1551E-09	8.4315E-09	8.4315E-09
8.5600E-11	-1.7504E-10	8.5600E-11	-6.8856E-08	-9.1167E-08	-6.8856E-08
-2.2580E-11	-2.2573E-11	-2.2580E-11	8.4315E-09	9.1551E-09	8.4315E-09
8.5600E-11	-1.7504E-10	8.5600E-11	-6.8856E-08	-6.8856E-08	-9.1167E-08
-2.2580E-11	-2.2573E-11	-2.2580E-11	8.4315E-09	8.4315E-09	9.1551E-09

References

[1] Update of Service Experience of HV Underground and Cable Systems, *CIGRE Technical Brochure 379*, April 2009.

[2] N. Momose, H. Suzuki, S. Tsuchiya, T. Watanabe, "Planning and Development of 500 kV Underground Transmission System in Tokyo Metropolitan Area," *CIGRE Session 1998*, 37-202.

[3] *Assessment of the Technical Issues relating to Significant Amounts of EHV Underground Cable in the All-island Electricity Transmission System*, (available on the web) Tokyo Electric Power Company, November 2009, http://www.eirgrid.com/media/Tepco%20Report.pdf.

[4] M. Rebolini, L. Colla, F. Iliceto, "400 kV AC new submarine cable links between Sicily and the Italian mainland. Outline of project and special electrical studies," *CIGRE Session 2008*, C4-116.

[5] L. Colla, S. Lauria, F. M. Gatta, "Temporary Overvoltages due to Harmonic Resonance in Long EHV Cables," *IPST 2007*, http://www.ipst.org /techpapers/2007/ipst_2007/papers_IPST2007/Session16/233. pdf.

[6] *Technical report on the future expansion and undergrounding of the electricity transmission grid*, (available on the web) Energinet.dk, April 2008, http://www.energinet.dk/NR/rdonlyres/CC966C3A-FE78-41D8-9D C7-6B455210B502/0/TechnicalReportSummary.pdf.

[7] N. Nagaoka, A. Ametani, "Transient Calculations on Crossbonded Cables," *IEEE Trans. on Power Apparatus and Systems*, vol. PAS-102, no. 4, April 1983.

[8] A. Ametani, Y. Miyamoto, N. Nagaoka, "An Investigation on a Wave Propagation Characteristic on a Crossbonded Cable," *IEEJ Trans. PE* , vol. 123-B, no.3, pp. 395-401, March 2003

[9] Stephen H. Hall, Howard L. Heck, *Advanced Signal Integrity for High-Speed Digital Designs*, Wiley-IEEE Press, March 2009

[10] A. Ametani, *Distributed-Parameter Circuit Theory*, Corona Pub. Co., 1990 (in Japanese).

[11] A. Ametani, "A study of cable transient calculations, Part II Transient calculations," *Science and Engineering Review of Doshisha University*, vol. 24, no. 2, pp. 119-127, July 1983.

Teruo Ohno (M'2006) received the B.S. degree from the University of Tokyo, Tokyo, and the M.S. degree from the Massachusetts Institute of Technology, Cambridge, both in electrical engineering, in 1996 and 2005, respectively.
Since 1996 he has been with the Tokyo Electric Power Company, Inc, where he is currently involved in studies on protection relays and special protection schemes. Currently, he is also studying PhD at the Institute of Energy Technology, Aalborg University. He is a secretary of Cigré WG C4.502, which focuses on technical performance issues related to the application of long HVAC cables. He is a member of IEEE and IEEJ (The Institute of Electrical Engineers of Japan).

Claus Leth Bak (M'1994, SM'2008) was born in Århus in Denmark, on April 13, 1965. He graduated from High School in Århus and studied at the Engineering College in Århus, where he received the B.Sc. with honors in Electrical Power Engineering in 1992. He pursued the M.Sc. in Electrical Power Engineering with specialization in High Voltage Engineering at the Institute of Energy Technology (ET) at Aalborg University (AAU), which he received in 1994. After his studies he worked with Electric Power Transmission and Substations with specializations within the area of Power System Protection at the NV Net Transmission Company. In 1999 he got employed as an Assistant Professor at ET-AAU, where he is holding a Professor position today. His main research areas include Corona Phenomena and audible noise on Overhead Lines, Power System Transient Simulations, Power System Protection and Offshore Transmission Networks. He works as a Consultant Engineer for electric utilities, mainly in the field of Power System Protection. He has supervised app. 20 M.Sc. theses, 10 B.Sc. theses and 8 PhD's. Claus Leth Bak teaches and supervises at all levels at AAU and he has a very large teaching portfolio. He is the author/coauthor of app. 70 publications. He is a member of Cigré C4.502, Cigré SC C4 and Danish Cigré National Committee. He is an IEEE senior member.

Akihiro Ametani (M'1971, SM'1983, F'1992, LF'2010) received the Ph.D. degree from UMIST, Manchester in 1973. He was with the UMIST from 1971 to 1974, and Bonneville Power Administration to develop EMTP for summers from 1976 to 1981. He has been a professor at Doshisha University since 1985 and was a professor at the Chatholic University of Leaven, Belgium in 1988. He was the Director of the Institute of Science and Engineering from 1996 to 1998, and Dean of Library and Computer/Information Center in Doshisha University from 1998 to 2001. He wa a Vice-President of IEE Japan in 2003 and 2004. Dr. Ametani is a Chartered Engineer in U.K., a Fellow of IET, Life Fellow of IEEE, and a Distingulshed member of CIGRE. He was awarded a D.Sc. (higher degree in UK) from the University of Manchester in 2010.

Wojciech Wiechowski (M'2008, SM'2008) received the M.Sc. degree from Warsaw University of Technology, Poland in 2001 and the Ph.D. degree in the area of harmonic analysis from Aalborg University, Denmark in 2006. From 2001 to 2002 he worked for HVDC SwePol Link as a Technical Executor. In the period from 2002 to 2006 he was with the Institute of Energy Technology, Aalborg University, first as a PhD Student and later as an Assistant Professor. In the period from 2006 to 2010 he was with the Development Department of the Danish TSO Energinet.dk where he was responsible for the cable technology R&D activities. In 2010 he established his own consultancy in electrical power engineering called WTW Power Solutions. He is the initiator and convener of the Cigré WG C4.502 "Power system technical performance issues related to the application of long HVAC cables", member of Cigré WG B1.30 "Cable System Electrical Characteristics", member of the Scientific and Technical Committee of Jicable'11 conference and a Senior Member of IEEE. He is an author and co-author of more than 30 scientific publications.

Thomas Kjærsgaard Sørensen (M'2011) received the M.Sc. degree from the Technical University of Denmark (DTU) in 2006 and the Ph.D. degree in the area of High Voltage Engineering also from DTU in 2010. Since 2010, he has been employed in the Grid Planning at the Danish TSO Energinet.dk. His main area of interest is power system transients simulations and insulation coordination studies with focus on system with large shares of cables and combined overhead line and cable systems.